G.KARATAŞ

MODELING AND MEASUREMENT OF MULTIPLE HUMAN BODY SHADOWING AT 28 GHz.

THE GRADUATE SCHOOL OF NATURAL AND APPLIED SCIENCES
OF
ATILIM UNIVERSITY

GÖKHAN KARATAŞ

A MASTER OF SCIENCE THESIS
IN
THE DEPARTMENT OF ELECTRICAL AND ELECTRONICS ENGINEERING

JULY 2020

ATILIM UNIVERSITY 2020

MODELING AND MEASUREMENT OF MULTIPLE HUMAN BODY SHADOWING AT 28 GHz.

A THESIS SUBMITTED TO
THE GRADUATE SCHOOL OF NATURAL AND APPLIED SCIENCES
OF
ATILIM UNIVERSITY

BY

GÖKHAN KARATAŞ

IN PARTIAL FULFILLMENT OF THE REQUIREMENTS
FOR
THE DEGREE OF MASTER OF SCIENCE
IN
THE DEPARTMENT OF
ELECTRICAL AND ELECTRONICS ENGINEERING

JULY 2020

Approval of the Graduate School of Natural and Applied Sciences, Atilim University.

_____

Prof. Dr. Ali KARA
Director

I certify that this thesis satisfies all the requirements as a thesis for the degree of **Master of Science in Electrical and Electronics Engineering Department, Atilim University**.

_____

Assoc. Prof. Dr. Kemal Efe ESELLER
Head of Department

This is to certify that we have read the thesis MODELING AND MEASUREMENT OF MULTIPLE HUMAN BODY SHADOWING AT 28 GHz. submitted by GÖKHAN KARATAŞ and that in our opinion it is fully adequate, in scope and quality, as a thesis for the degree of Master of Science.

_____

Prof. Dr. Ali KARA
Supervisor

Examining Committee Members:

Asst. Prof. Dr. Özgür Ergül
Electrical and Electronics Eng. Dept., Gazi University _____

Prof. Dr. Ali Kara
Electrical and Electronics Eng. Dept., Atilim University _____

Prof. Dr. Çiğdem S. Gürel
Electrical and Electronics Eng. Dept., Hacettepe University _____

Prof. Dr. Elif Aydın
Electrical and Electronics Eng. Dept., Atilim University _____

Assoc. Prof. Dr. Ömer Karal
Electrical and Electronics Eng. Dept., AYBU _____

Date: 22/07/2020

I hereby declare that all information in this document has been obtained and presented in accordance with academic rules and ethical conduct. I also declare that, as required by these rules and conduct, I have fully cited and referenced all material and results that are not original to this work.

Gökhan KARATAŞ

Signature:

ABSTRACT

MODELING AND MEASUREMENT OF MULTIPLE HUMAN BODY SHADOWING AT 28 GHz.

Karataş, Gökhan

M.S., Department of Electrical and Electronics Engineering

Supervisor: Prof. Dr. Ali KARA

July 2020, 44 pages

This thesis represents the simplified human body models and their comparison with measurement results to characterize the effects of the scattering human bodies near the indoor link. The studies were performed while the human body was entirely blocking the link between the transmitter to the receiver. The measurements were conducted at 28 GHz., which has great importance for the fifth-generation (5G) wireless systems. Additionally, the theoretical background of the human body modeling and mechanisms of wave propagation were presented with other required concepts to comprehend the studies briefly. The effects of the scattering human bodies were simulated using models such as double knife-edge diffraction (DKED) and geometric theory of diffraction (GTD) through ray-tracing. These models were exploited from underlying wave propagation mechanisms such as reflection and diffraction during the simulations. Moreover, the simulations were performed for scenarios; one and two human bodies as scattering objects while the link is fully blocked by another human body separately.

Furthermore, these simulations were compared with the corresponding laboratory measurements, and promising results were obtained. The simplified human body models are compatible with the measurement results. It is considered that these models will be rewarding while designing the wireless channel for millimeter-wave (mmWave).

The new studies within the frame of this thesis could be developed for the future allocations in mmWave bands. Besides, simplified models could be extended to characterize the effects of multiple human bodies for different deployments.

Keywords: 5G, millimeter-wave, ray-tracing, double knife-edge diffraction, multiple human body blockage, human body shadowing, geometric theory of diffraction, human body models.

ÖZ

28 GHz'DE ÇOKLU İNSAN VÜCUDU GÖLGELEMESİNİN ÖLÇÜLMESİ VE MODELLENMESİ

Karataş, Gökhan
Yüksek Lisans, Elektrik ve Elektronik Mühendisligi
Tez Yöneticisi: Prof. Dr. Ali KARA

Temmuz 2020, 44 sayfa

Bu tez, iç mekân bağlantısı yakınlarında bulunan saçılmış insan vücutlarının etkilerini karakterize etmek amacıyla basitleştirilmiş insan vücudu modellerini ve onların ölçüm sonuçlarıyla kıyaslamasını sunmaktadır. Çalışmalar; insan vücudu tamamen verici ile alıcı arasındaki bağlantıyı engellerken gerçekleştirilmiştir. Ayrıca, ölçümler kablosuz beşinci nesil (5G) sistemler için büyük öneme sahip olan 28 GHz'de yapılmıştır. Ek olarak, insan vücudu modelleme ve dalga yayılım mekanizmalarının teorik arka planı ile çalışmaları kavramak için gerekli diğer kavramlardan kısaca bahsedilmiştir. Saçılmış halde bulunan insan etkileri, çift bıçak kenarı kırınımı (DKED) ve ışın izleme yoluyla geometrik kırınım teorisi (GTD) gibi modeller kullanılarak benzetimler yapılmıştır. Benzetimler esnasında, modellerde yansıma ve kırınım gibi temel dalga yayılma mekanizmalarından faydalanılmıştır. Benzetimler; bağlantı tamamıyla insan tarafından engellenmiş durumda iken saçılmış olarak bulunan bir ve iki insan vücudu senaryoları için ayrı ayrı gerçekleştirilmiştir.

Ayrıca, bu benzetimler ilgili laboratuvar ölçümleri ile karşılaştırılmış ve ümit verici sonuçlar elde edilmiştir. Basitleştirilmiş kırınım modellerinin ölçümlerle uyum içinde olduğu görülmüştür. Bu modellerin milimetre dalgaları (mmWave) için kablosuz kanal tasarlarken faydalı olacağı düşünülmektedir.

Diğer yandan, milimetre dalga bantlarında yakın gelecekte yapılacak tahsisler için bu tez çerçevesinde yeni çalışmalar geliştirilebilir. Ayrıca, basitleştirilmiş modeller, çoklu insan vücudunun farklı yerleşimlerdeki etkilerini karakterize etmek için genişletilebilir.

Anahtar Kelimeler: 5G, milimetre dalga, ışın izleme, çift bıçak kenarı kırınımı, çoklu insan engeli, insan vücudu gölgeleme, geometrik kırınım teorisi, insan vücudu modelleri.

To My Family..

ACKNOWLEDGMENTS

I would like to express my deepest gratitude to my supervisor, Professor Ali Kara, for his excellent guidance, consistent support, and encouragement throughout my thesis. He spent a great deal of time and effort on this work. He always supported whenever I need without hesitation.

Besides, I would like to thank Asst. Prof. Yaser Dalveren for his advice, support, and guidance.

Furthermore, I would like to express my sincere thanks to my head of the department in the Information and Communication Technologies Authority (BTK), Afşin Büyükbaş, who provided the necessary convenience and understanding throughout my thesis.

Also, I would like to thank İrem Kibar, Oğuzhan Öztürk, Halil Karataş, Adramane Assoumana, and Sinem Yabaş for their sincere support and encouragement throughout my thesis.

Finally, I must present my sincere gratitude to my family members for their patience and encouragement throughout my thesis. This success would not be possible without them.

TABLE OF CONTENTS

LIST OF TABLES

TABLES

LIST OF FIGURES

FIGURES

LIST OF SYMBOLS/ABBREVIATIONS

MmWave	Millimeter waves
2G	Second Generation
5G	Fifth Generation
IoT	Internet of Things
D2D	Device to Device
M2M	Machine to Machine
LOS	Line of Sight
NLOS	Non-Line of Sight
GHz	Giga Hertz
TM	Transverse Magnetic
TE	Transverse Electric
DB	Decibel
GTD	Geometric Theory of Diffraction
UTD	Uniform Theory of Diffraction
KED	Knife Edge Diffraction
DKED	Double Knife Edge Diffraction
RF	Radio Frequency
IMT	International Mobile Telecommunications
m	Meter

CHAPTER 1

INTRODUCTION

Currently, the prevailing changes and developments not only have been seen in all realms of the science but also they have given the name to the current historical period as an information era. Invented technologies facilitate our life without a doubt. It is seen that their advantages are stemmed from the methods they are using now. It could be considered that the accessibility of the internet is the main reason for the changes over the methods. Therefore, the supremacy of the internet has affected the circulation speed of the data and the methods in all areas, respectively. Although prior wireless cellular generations did not comprise the data transfer until GPRS of a second-generation cellular system (2G) [1], the data transfer through the internet is an integral part of contemporary wireless cellular communication. Especially when considering the fifth-generation cellular system (5G) that will be the primary cellular system soon, cellular networks could not be considered without the internet. Moreover, upcoming applications of 5G, such as IoT, D2D, M2M, smart homes, augmented reality, could not be separated from data transfer through the internet [2]. On the other hand, these expectations mainly depend on adequate transmission speeds and low latency apart from other upcoming features [3]. Therefore, these new expectations will bring challenges to be dealt with inevitable. These challenges will arise from the necessity of additional bandwidth [4]. For example, internet-connected devices will increase the level of internet traffic apart from the internet user human population. However, the electromagnetic spectrum is regarded as a limited natural source. The frequency demands of the new implementations could not be provided due to the unsuitable reallocation in the lower frequencies. Accordingly, the electromagnetic spectrum urges us to exploit the millimeter-wave bands for brand-new technologies.

The millimeter-wave bands (mmWave bands) are named for the electromagnetic waves, which have the property of the frequency range between the 30-300 GHz. The utilization of the mmWave bands has been stemmed from the scarcity of the bandwidth in the lower frequency bands. However, the characteristics of mmWave also have crucial importance over the propagation scenarios and implementations.

Besides, in the World Radiocommunication Conference (WRC-19), which was organized by International Telecommunication Union in Sharm in El-Sheikh in 2019, additional frequency bands in mmWave are allocated for IMT systems for the future mobile demands. These bands are 24.25-27.5 GHz., 37-43.5 GHz., 45.5-47 GHz., 47.2-48.2 GHz., and 66-71 GHz. [5].

1.1 Research Background

The IoT will increase bandwidth usage. The demands for the new bandwidth to diminish the data traffic density will be provided from the mmWave bands. Because of this reason, the propagation scenarios over the mmWave bands have crucial importance in wireless communication. To figure out the propagation characteristics of the mmWave bands will give us precious knowledge to be ready for the challenges while designing the cellular network.

Unlike the lower frequency bands, mmWave bands are easily affected by the atmospheric environment due to their characteristics. In addition, building penetration of mmWave bands is remarkably low and limited. The circumstances, such as shadowing, can cause significant signal attenuation over the propagation channel in mmWave bands. Consequently, it is seen that mmWave bands are more sensitive to blockage from scattering objects [6].

Besides, the mmWave bands have less coverage than the lower frequency bands due to their small wavelengths and decreased signal strengths in high frequencies [7]. On the other hand, easily affected nature leads to increased frequency reuse ratio. In this context, mmWave bands are considered for indoor communication systems and distance-limited implementations for 5G due to decreased cell coverage and increased frequency reuse ratio [8].

Moreover, the Friis equation, which indicates the signal path loss directly proportional to the square of the frequency, proves the extremely affected nature of the mmWave bands [9].

The shadowing should be considered another challenge for indoor applications at mmWave bands because studies indicated that shadowing loss that was stemming from the human body was approximately 20-35 dB [11]. In this context, the people could be considered the most effective shadowing object in the environment due to its dynamic status over the propagation line. Therefore, various studies were carried out about predicting and modeling over the human body shadowing for optimizing the wireless networks in the environments, and there is still a lot to do.

On the other hand, the diffraction and reflection contributions to received signals occur from the scattering objects. These contributions could be taken into account in a supportive manner for indoor environments [10]. It will be worthwhile to characterize the effects of these contributions before planning and designing the usage of mmWave bands.

1.2 Literature Review

There are various papers in the literature that tried to model and characterize the multiple human body shadowing. These papers tried to obtain useful information to comprehend the propagation channel during the human presence.

This paper [12] consists of human body shadowing and the scattering objects to characterize the mmWave bands behavior at 28 GHz. The characterization benefited from the reflection and diffraction mechanisms of wave propagation in the indoor environment. The specular reflection model and double knife-edge diffraction model were applied while a person entirely blocked the LOS propagation between the transmitter and receiver. Furthermore, the simulation results were compared with the laboratory measurement results to indicate the compatibility of the models. The metallic reflector and human body were positioned at specified intervals to predict the attenuation sourced by the scattering objects. The effects of reflection and diffraction mechanisms were tried to be seen on the receiver power.

The encouraging results were obtained about the feasibility of the double knife-edge diffraction model and specular reflection model for characterizing the signal propagation in mmWave bands.

Another paper about the propagation model concentrated on the path loss while taking into account the shadowing loss in congested environments. The studies were carried out by using the frequencies ranging from the 4.7 GHz. and 66.5 GHz. The measurements were taken in the ticket gate, which used by around 140.000 people in a day. Furthermore, there was nothing but people between the transmitter and receiver points. The results were encouraging and reflecting the high accuracy with the applied model [13].

The path loss model was applied to simulate the human body shadowing loss in a crowded area at 4.7 GHz. and 26.4 GHz. to characterize the human body shadowing. The measurement results and simulation results were compared, and promising outcomes were obtained [14].

Various models were used to characterize the radio propagation in 28 GHz. The propagation environment was tried to be modeled by double knife-edge diffraction model and multiple knife-edge diffraction model. While evaluating the effects of diffraction on models, the Fresnel diffraction method was used. Measurements were taken while the human was positioned over the predetermined places through the LOS path and the path that was perpendicular to the LOS path separately. The measurement results indicated that the gains were ranging from 15.62 dB to -6.29 dB. The measurement results were compared with the simulation results of the double knife-edge and multiple knife-edge models. The experiments concluded that the multiple knife-edge model simulation results were more familiar with the measurement results than simulation results of the double knife-edge model [15].

In [16], received power was tried to be characterized statistically in the time domain while the human was either in slow-motion or the static presence at the LOS propagation in 60 GHz. After obtaining the measurement results, it was seen that received power fluctuations behaved similarly to the Gaussian statistical model. In addition, results indicated that the static body caused longer attenuate time duration than the slow motion.

For characterizing the human body shadowing loss, modified double knife-edge model was developed. Additionally, this model exploited from the antenna radiation pattern in 73 GHz. [17]. The experiment was carried out at a distance of 5.0 m and human was positioned at every 0.5 m interval. Signal attenuations were measured while using the directional antennas. The measurement results were compared with the modified double knife-edge model and double knife-edge model of the METIS Project. Consequently, it was seen that the modified double knife-edge model was more compatible with the laboratory measurement than the double knife-edge model generated by the METIS Project in terms of results.

The extended calculation model was applied to the experiments to predict the shadowing loss of human in motion at 60 GHz. The human body approximated as a rectangular shape. In addition, three knife-edge paths considered during the calculation of shadowing loss. Results were obtained from the simulations and laboratory measurements were compared. Consequently, the simulations indicated the shadowing loss of approximately 20 dB and results were compatible with the model results [18].

In [19][20], the human body approximated as conducting circular cylinder and exploited from the GTD. Measurements were obtained at 10.5 GHz. within the predetermined positions at 28 GHz. Human bodies were admitted as a perfectly conducting cylinder, then the effects of human bodies were analyzed. The promising results were obtained.

In this paper [21], received power was tried to be modeled through the classification of multipath contributions through ray-tracing. Since cities consist of buildings of various heights and densely human body occupations, it is not easy to predict the signal attenuation along the LOS and NLOS paths in city canyons. The paper divided the urban radio propagation into three main groups, which were LOS, one turn-NLOS and two turn-NLOS. Moreover, the measurement results were compared with the simulation results of models. These models indicated promising results for the prediction of the total received power. Furthermore, it was seen that the ray-tracing method could be utilized for the indoor human body models like the rectangular blade model [33].

1.3 Aim and Objectives of the Study

Current mmWave band allocations indicated that the mmWave bands consist of the unlicensed and suitable vast amount of frequency bands [5]. In addition, it is seen as the primary solution for the overcrowded data traffic shortly, stemming from the upcoming applications. Due to the limited propagation properties of mmWave bands, these bands will be mostly used for the indoor operations or distance-limited operations. In my opinion, there are not enough works to characterize the effects of the human body in mmWave bands and for 28 GHz. The human body is considered the fundamental element for indoor communication links in terms of shadowing. Most of the countries in the world consist of more than two living people considering the household size [22]. Accordingly, the multiple human body shadowing should be taken into account for more accurate characterization in the indoor environment. In our model, while one human body was blocking the LOS propagation, another two human bodies were positioned as scattering objects. Furthermore, during the characterization, the DKED and the GTD Models were exploited in simulations. The simulation models had promising results with the measurements. The results may be encouraging for the researchers who would like to make studies about the effects of the human body at indoor scenarios in mmWave bands.

1.4 Thesis Structure

This thesis consists of five chapters. Chapter 1 is the introduction chapter and consists of a research background, literature review, aims and objectives, thesis structure. Furthermore, Chapter 2 contains the theoretical background of signal propagation and human body models. Moreover, Chapter 3 consists of the measurement setup and experiment models in detail. Chapter 4 represents the results of the measurements and simulations. Finally, Chapter 5 is the conclusion chapter.

CHAPTER 2

HUMAN BODY MODELING AND SIGNAL PROPAGATION

The use of mmWave bands for the upcoming 5G networks will require delicate studies over the signal behaviors to characterize the channel. The studies should be done over the transmitter power, receiver power, and their correlations to characterize the channel in communication. This will account for the effects of the human bodies as scattering objects around the propagation link.

Some key concepts should be deeply involved, namely free space propagation, path loss, or path gain, to figure out the behavior of the signal in the wireless channel. Besides, understanding the mechanisms of wave propagation, such as diffraction, reflection, and scattering, which have great importance during the modeling of the human bodies in the environment, will be rewarding. On the other hand, being familiar with these topics will help to perceive the human body models and calculation of simulations in the following chapters. In this chapter, the theoretical background of propagation and mechanisms are presented, and other required concepts to comprehend the thesis are introduced.

2.1 Channel Modeling

The channel modeling is commonly divided into three main classes as Physical, Empirical, and Statistical Models. The Physical Models benefit from Geometric Optics, which consists of exact physical issues like scattering, diffraction, and reflection. On the other hand, the Empirical Models are based on empirical measurements over a particular range of frequencies along with a particular distance for particular environments.

These methods generally are used in the performance analysis and Okumura-Hata Model, Walfish-Bertoni Model, Piecewise Linear Model can be considered as common models among other Empirical Models [9]. The statistical models are used to characterize the predetermined environments, which consist of complicated circumstances that could not be handled with the deterministic models. The statistical models depend on random time-varying responses, which can be calculated more easily through computers. On the other hand, these models have low accuracy than physical models. Since physical models have insights that are more accurate according to results, we concentrated on the physical channel models. Furthermore, common physical mechanisms of wave propagation were taken into account during the calculation of applied models.

2.2 Free Space Propagation

The communication systems consist of three main blocks named transmitter, channel, and receiver. In the transmitter block, the information is converted to an electrical signal then to the radio waves via antennas. Finally, the information is transferred to the receiver through the channel. Besides, air could be considered as a channel for wireless communications. On the other hand, the receiver reciprocally turns the radio waves into information via antennas and converters.

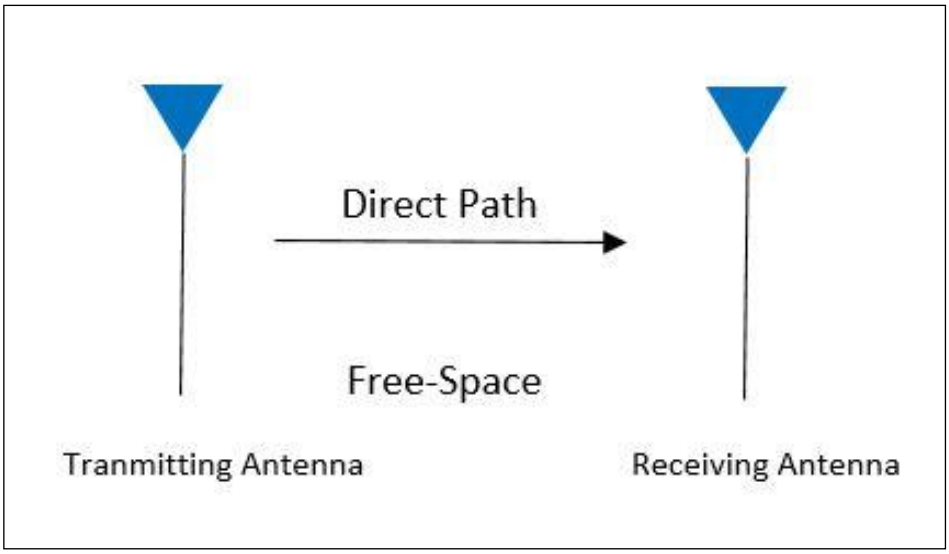

Figure 2.1: Free space propagation

The free space propagation model is an assumption allowing us to analyze the effects of distance on the receiver side. This model is based on thought that there is nothing but distance between the transmitter and receiver, as given in Figure 2.1, and admits that the antennas radiate omnidirectionally in the LOS path.

2.3 Path Loss, Path Gain and Shadowing in Large Scale Fading

Path loss, shadowing, and multipath should be accounted for accurate characterization when modeling the wireless communication environment. The fading of the signal could be stemmed from various reasons such as noise, interference, impediment of the channel due to obstacles. Therefore, the signals change in phase and amplitude during the propagation over paths. The fading can be categorized according to the character of the propagation paths. The fading that is caused by attenuation of the signal over large distances is named large-scale fading; on the other hand, small-scale fading concentrates on the fluctuations on the signal within the short durations or distances. [32]. Path loss, shadowing, and multipath effects along with the distance are illustrated in Figure 2.2.

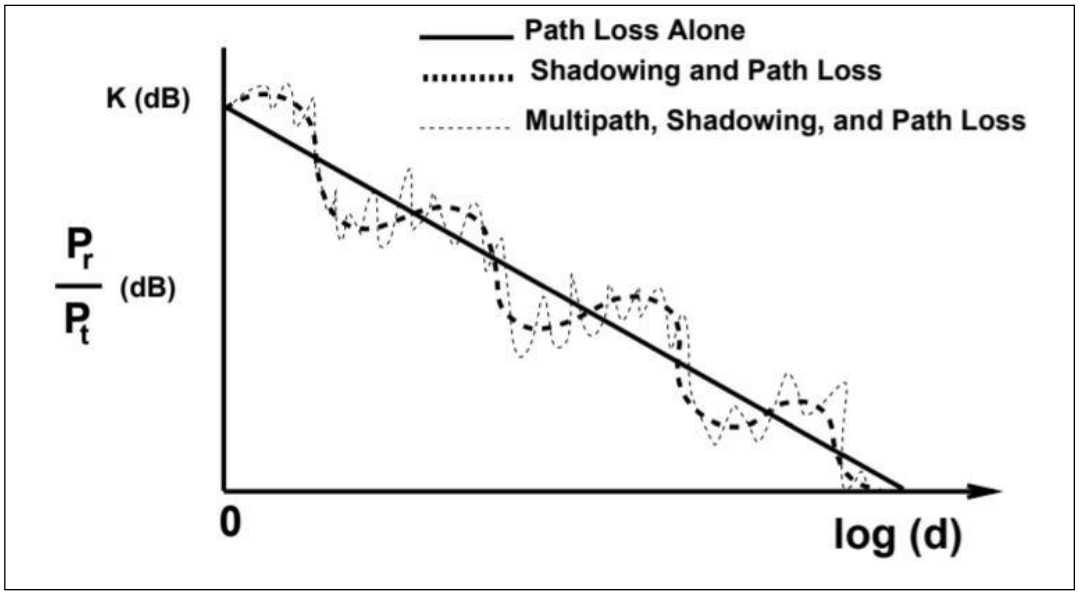

Figure 2.2: Path Loss, shadowing and multipath effects over distances [35]

The path loss of the channel can be defined as the ratio of the transmitted signal power to received signal power. Path loss is a positive quantity and only demonstrates the reduction in the signal power. Furthermore, path loss is primary component of the link budget [23]. Path gain is the reversed sign of the path loss and is demonstrated with the minus sign of the path loss. The path gain can be presented as in Equation 2.1 below.

$$PG\ (dB) = -PL = 10\log 10\left(\frac{Pr}{Pt}\right) \tag{2.1}$$

Where Pr and Pt denote the received signal power and transmitter signal power respectively.

Furthermore, the free-space path loss between the two isotropic omnidirectional antennas depends on the wavelength of the transmission line due to the effective area of the antennas [23]. It can be calculated by

$$FSPL\ (dB) = 20\log\left(\frac{4\pi d}{\lambda}\right) \tag{2.2}$$

Where

$$\lambda = \frac{c}{f} \tag{2.3}$$

Besides, the ratio of the transmit power to the receiver power also corresponds to the free-space path loss. λ is given in Equation 2.3 denotes the wavelength of the signal, which is the ratio of the speed of light to the frequency.

In case of the using directional antennas, we should take into account the antenna gains as well as free-space path loss to predict the receiver power. The Friis transmission equation is given in Equation 2.4, represents the ratio of the transmitted and received power.

$$P_R(dB) = P_T(dB) + G_{Tx}(dB) + G_{Rx}(dB) - FSPL(dB) \quad (2.4)$$

Where $G_{Tx}(dB)$ and $G_{Rx}(dB)$ denote the transmitter antenna gain and receiver antenna gain, respectively.

Another large-scale fading phenomenon is shadowing, which is arisen by the blockage of the LOS propagation path. Accordingly, only diffracted rays of a signal can contribute to the received power in the shadowing region.

2.4 Physical Channel Modeling and Propagation Mechanisms

Electromagnetic waves have a complicated nature that consists of various propagation mechanisms such as reflection, diffraction, and scattering. These mechanisms are encountered in urban areas due to the impediment of the LOS propagation in the channel. Thanks to these mechanisms, electromagnetic waves travel along the various paths that are incorporated at the receiver side. These paths have great impacts over the wireless channel modeling.

Electromagnetic waves, generated from the antenna source, propagate in the form of spherical waves within different polarizations and phases far from the antenna regions. Furthermore, amplitudes of the spheres are inversely proportional to the distance [9].

2.4.1 Reflection Mechanism

Reflection is a crucial phenomenon, and one of the fundamental mechanisms for physical channel modeling. Especially to comprehend the ground effect on the channel, reflection should be incorporated for more realistic channel modeling. When electromagnetic waves travel over one medium to another medium with different matter properties, reflection occurs. If the electromagnetic waves incident from the dielectric medium, they will transmit some amount of their energy to the medium. Besides, the remaining energy will be reflected from the medium due to the dielectric constant of the medium.

On the other hand, if the electromagnetic waves encounter the perfect conductor material, all energy will be reflected from the medium. The reflection coefficients depend on the TM and TE polarization of the transmission. Besides, angle of the incidence along with the dielectric properties of the matters from Snell's Law should be taken into account. Snell's Law is given in Equation 2.5

$$\sin\theta = \sin\theta_R = \sqrt{\varepsilon_r} * \sin\theta_T \tag{2.5}$$

Where θ, θ_R and θ_T denote the received angle of incidence, angle of the reflected wave, and angle of the transmitted wave, respectively. Hence, the reflection coefficient for the TE polarization can be calculated as

$$\Gamma_E = \frac{\cos\theta - \sqrt{\varepsilon_r} * \cos\theta_T}{\cos\theta + \sqrt{\varepsilon_r} * \cos\theta_T} \tag{2.6}$$

Moreover, reflection coefficient for the TM polarization can be calculated by

$$\Gamma_H = \frac{\sqrt{\varepsilon_r} * \cos\theta - \cos\theta_T}{\sqrt{\varepsilon_r} * \cos\theta + \cos\theta_T} \tag{2.7}$$

2.4.1.1 Plane Earth Model (Two-Ray Model)

Because of its shape, the Earth has effects on the electromagnetic waves, excluding very short distances between the transmitter and receiver. The Two-Ray Model was introduced to predict the path losses over LOS propagation of electromagnetic waves. For the distances less than tens of kilometers, we can assume the Earth as a flat surface, and we can make the approximations over the propagation environment depending on this assumption. The Plane Earth Model consists of two rays; one is the reflected ray from the ground other is the direct ray between the transmitter and receiver.

These rays aim to obtain the received power more accurately to see the effects of the environments through including the ground effects. Consequently, the total power can be calculated by the coherent summation of the two electrical fields that are occurred over the two-ray path. The Two-Ray Model is illustrated in Figure 2.3.

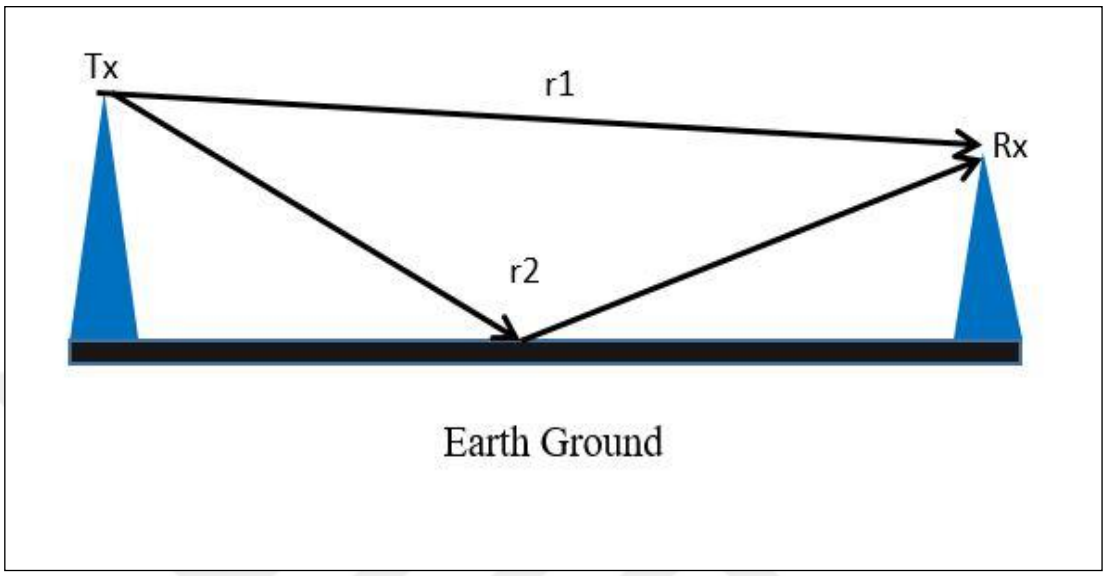

Figure 2.3: Plane Earth Model (Two-Ray Model)

Hence, the path gain due to the ground reflected ray and direct ray can be obtained by Equation 2.8

$$PG = \left(\frac{\lambda}{4\pi r}\right)^2 \left|\frac{e^{-jkr1}}{r1} + \Gamma_H(\theta)\frac{e^{-jkr2}}{r2}\right|^2 \quad (2.8)$$

Where *r* is the unfolded path distance from transmitter antenna to receiver antenna and r_1 is the distance of LOS ray from transmitter antenna to receiver antenna.

On the other hand, r_2 denotes total unfolded path distance of the reflected signal between receiver and transmitter antenna at the desired angle. $\Gamma_H(\theta)$ denotes the reflection coefficient of the ground for the horizontal polarization. Lastly, *k* denotes the wavenumber of the wave.

2.4.2 Diffraction Mechanism

The diffraction is seen as one of the leading mechanisms to apply for predicting the effects of human body shadowing over the received power in channel modeling. The diffraction occurs when the obstacle or human body blocks the LOS path. The diffraction mechanism was used by many human body shadowing models [12] [15] [17] [19]. Furthermore, diffraction is the mechanism that accounts for the traveling of the electromagnetic waves and their presence within the shadowing boundary.

The Huygens-Fresnel principle explains that the diffracted waves are second wave sources. These secondary wavelets occur during the diffraction, and they are contributing to the shadowed region. Moreover, diffracted fields represent cylindrical wave propagation characteristics in the near field [9]. The generated plane waves by the transmitter reach the receiver through bending around the obstacles without the LOS propagation.

The diffraction coefficient is one of the fundamental parameters for predicting the effects of the diffraction mechanism over the receiver power. Besides, the frequency of the propagation and incident angles are the other affecting properties for the diffraction coefficient. Usually, Geometric Theory of Diffraction and Knife-Edge Diffraction Modeling were taken as a basis to simulate the effects of the human body shadowing loss in the environment due to their accuracy instead of statistical human body models such as Gaussian Model [24] and Bayesian Model [25].

2.4.2.1 Knife-Edge Diffraction Model (KED)

The KED Model is the simplest diffraction model for predicting the attenuation of the signal when obstructions block the link. The obstruction is considered as a knife-like edge and is positioned between the transmitter and receiver, as given in Figure 2.4. The obstruction is considered to have infinite dimensions other than blade-like edges and is assumed not to allow the signal to pass. Accordingly, no signal is traveling through other edges.

Furthermore, it helps us during the assessment of the secondary wavelets that occurred from the knife-edge while modeling. Only contributions from the knife-edges should be taken into account during the assessments.

The diffraction loss can be calculated by dint of a single, dimensionless quantity that is named Fresnel-Kirchhoff diffraction parameter. Furthermore, the path gain or path loss can be determined by Fresnel integral, which is given in Equation 2.10. Meanwhile, the Fresnel-Kirchhoff parameter derived from the equation, which is given in Equation 2.9.

$$v = h\sqrt{\frac{2(d1+d2)}{\lambda(d1d2)}} \tag{2.9}$$

Where *h*, *d1* and *d2* denote the height of the obstruction, distances between the transmitter to obstruction and obstruction to receiver, respectively.

$$F_c(v) = \int_0^v \frac{e^{-i\pi s^2}}{2} ds = C(v) + jS(v) \tag{2.10}$$

Where, *C(v)* and *S(v)* denote the Fresnel cosine and sine integrals.

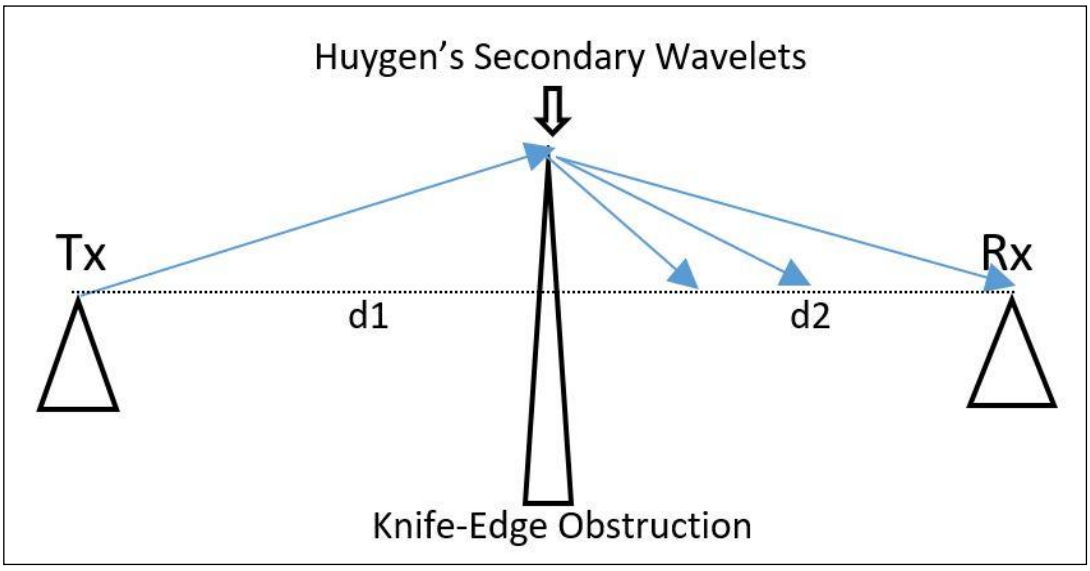

Figure 2.4: Knife-Edge Diffraction Model

Although it is not easy to calculate the attenuation of the signal, the KED model indicates the qualified approximations and insights about the signal attenuation without being involved in the irregular geometry of obstructions. Thanks to this model, we can assume the human body as a rectangular absorbing screen. Furthermore, many modified diffraction models were stemmed from the KED model, such as the METIS KED Model and the DKED Model.

2.4.2.1.1 METIS Knife-Edge Diffraction Model

The Mobile and wireless communications Enablers for the Twenty-twenty Information Society (METIS) developed the modified knife-edge diffraction model to determine the shadowing loss from the obstruction [27]. In this model, each blockage was considered as rectangular screen. The screen was positioned vertical and perpendicular to the propagation line between the transmitter and receiver. The shadowing loss occurred by the obstruction can be obtained by

$$L_{sh}(dB) = -20log_{10}(1-(Fh1+Fh2)(Fw1+Fw2)) \tag{2.11}$$

Where *Fh1, Fh2, Fw1, Fw2* denote the knife-edge diffraction for each edge and they were illustrated in Figure 2.5. These can be determined by

$$F = \frac{\tan^{-1}\left(\frac{-}{+}\frac{\pi}{2}\sqrt{\frac{\pi}{\lambda}(D1+D2-r)}\right)}{\pi} \tag{2.12}$$

The plus (+) sign is applied if the ray is in the LOS propagation and is shadowed by the obstruction, whereas minus sign (-) is used in case the ray is in the NLOS propagation. *D1* and *D2* are the projected distances and, *r* is the LOS path distance between the transmitter and receiver.

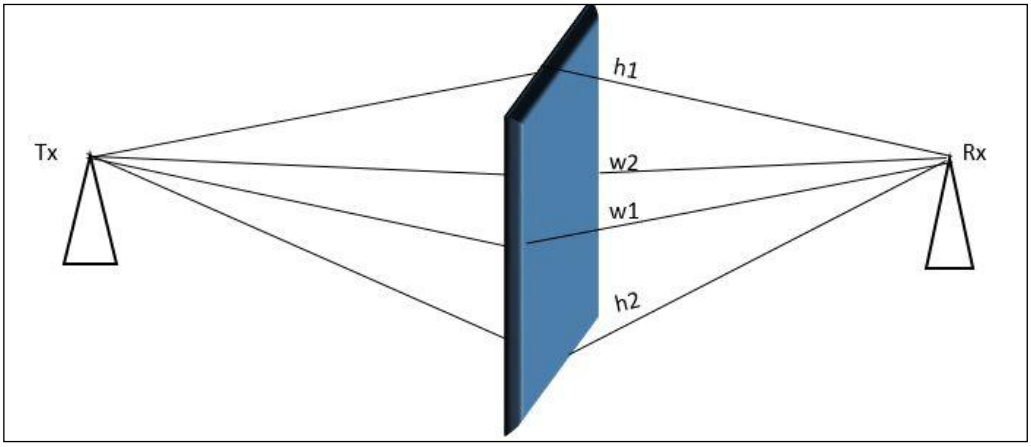

(a)

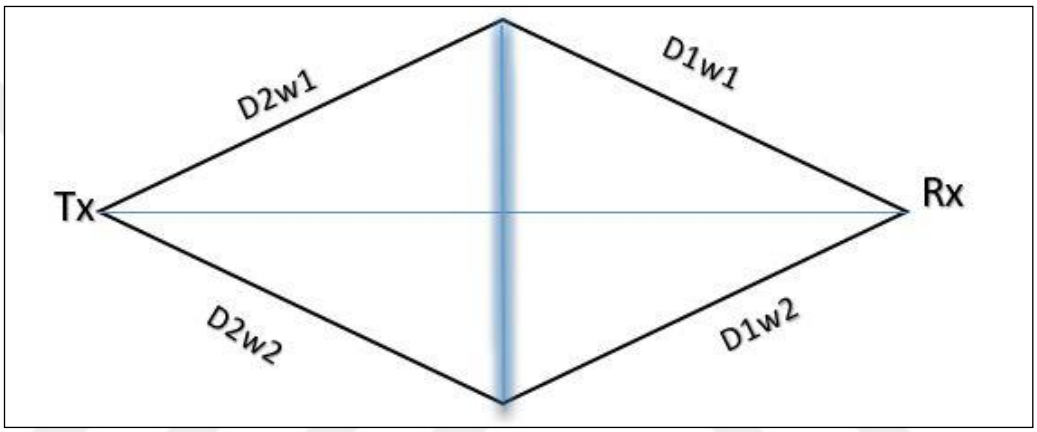

(b)

Figure 2.5: (a) 3D projection. (b) Top-down projection of METIS Model

2.4.2.1.2 Double Knife-Edge Diffraction Model

The DKED model is another modified knife-edge diffraction model for modeling the human body in the channel. The DKED model can be considered as the incorporation of two knife-edge models back to back. In this model, the human body is approximated as an absorbing rectangular screen and is illustrated in Figure 2.6. Although the diffracted rays occur from horizontal edges, the vertical edges do not allow any signal due to the assumption that they have infinite heights. Furthermore, some developments over the DKED model were performed by adding the antenna radiation pattern. This modified model was indicated promising simulation results with the measurement results [17].

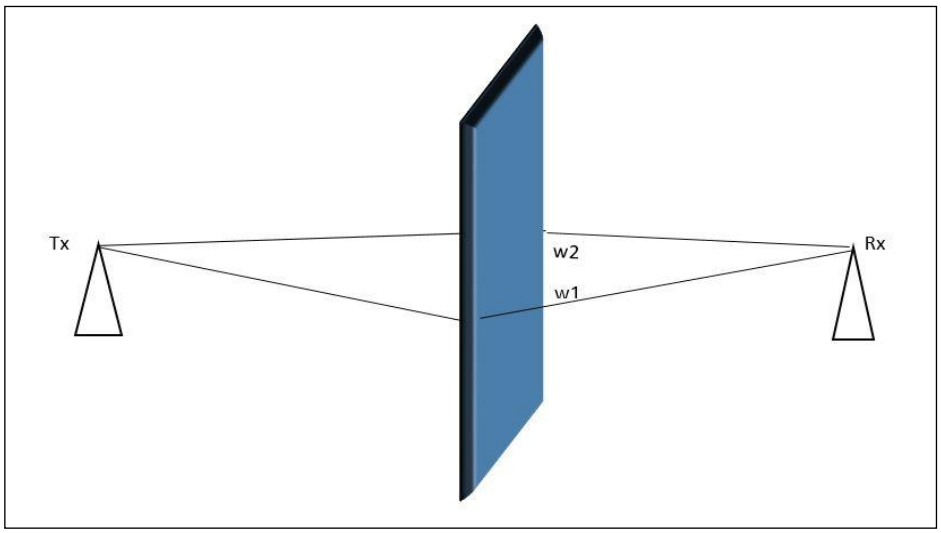

(a)

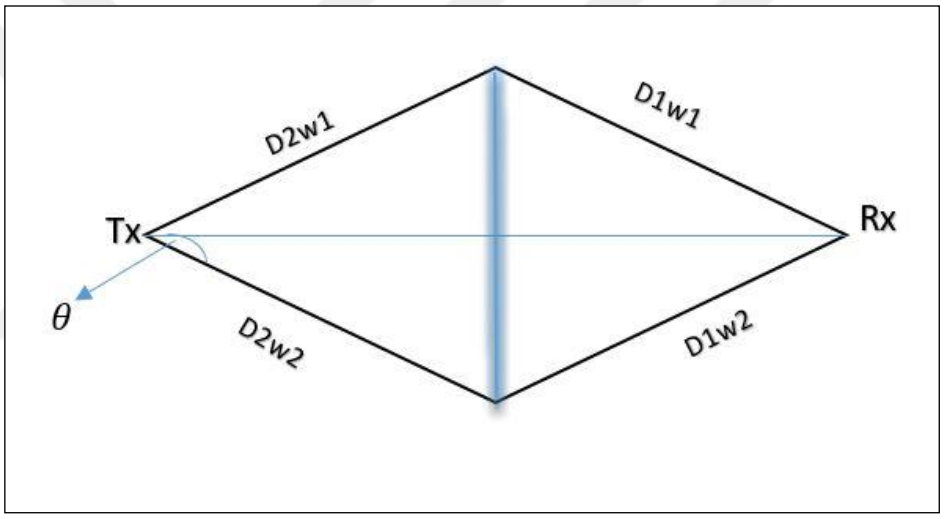

(b)

Figure 2.6: (a) 3D projection. (b) Top-down projection of DKED model

The shadowing loss occurred from the obstruction can be obtained by

$$L_{sh}(dB) = -20log_{10}\left|\left(\frac{1}{2} - Fw_1\right) * \sqrt{G_{Txw1}(\theta)} * \sqrt{G_{Txw2}(\theta)} + \left(\frac{1}{2} - Fw_2\right) * \sqrt{G_{Rxw1}(\theta)} * \sqrt{G_{Rxw2}(\theta)}\right| \quad (2.13)$$

Where $G_{Txw1}(\theta)$ and $G_{Rxw2}(\theta)$ are transmitter and receiver antenna boresight gains at the angle of θ that is indicated in Figure 2.6 (b) for the directional antennas. Fw_1 and Fw_2 indicate the electromagnetic field gains which are arising from diffraction. Besides, the diffraction from the horizontal edges can be calculated as

$$F_{w1,w2} = \frac{\tan^{-1}\left(\frac{-\pi}{+2}\sqrt{\frac{\pi}{\lambda}(D2_{w1,w2}+D1_{w1,w2}-r)}\right)}{\pi} \quad (2.14)$$

Besides, the distances, which are related to *D2* and *D1* are illustrated in Figure 2.6 (b).

2.4.2.2 Geometric Theory of Diffraction (GTD)

The GTD is the oldest and one of the most commonly used diffraction models. The GTD Model predicts the field strength accurately in the region away from the diffraction point. The GTD tries to interpret and characterize the incident rays that hit the surfaces, edges, or wedges. It exploits the geometric optics while obtaining the behavior of incident rays. In other words, the GTD is a developed version of geometric optics to characterize the diffraction in the environment. It represents the diffracted rays along with the usual rays of geometric optics [34]. Furthermore, the Cylindrical Model and the Rectangular Blade Model are the most commonly used GTD models to characterize the human body shadowing due to their accuracy and simplicity.

2.4.2.2.1 Cylindrical Model

The Cylindrical Model is regarded as a type of human body model under the GTD Models. It is seen that the Cylindrical Model was employed to simulate the effects of human body shadowing loss in many studies. In these studies, the human bodies were regarded as a perfectly conducting cylinder that does not contain any lateral wedges [19] [20] [26].

Besides, instead of using knife diffraction approximation, this method benefits from the surface diffraction approximations, as illustrated in Figure 2.7.

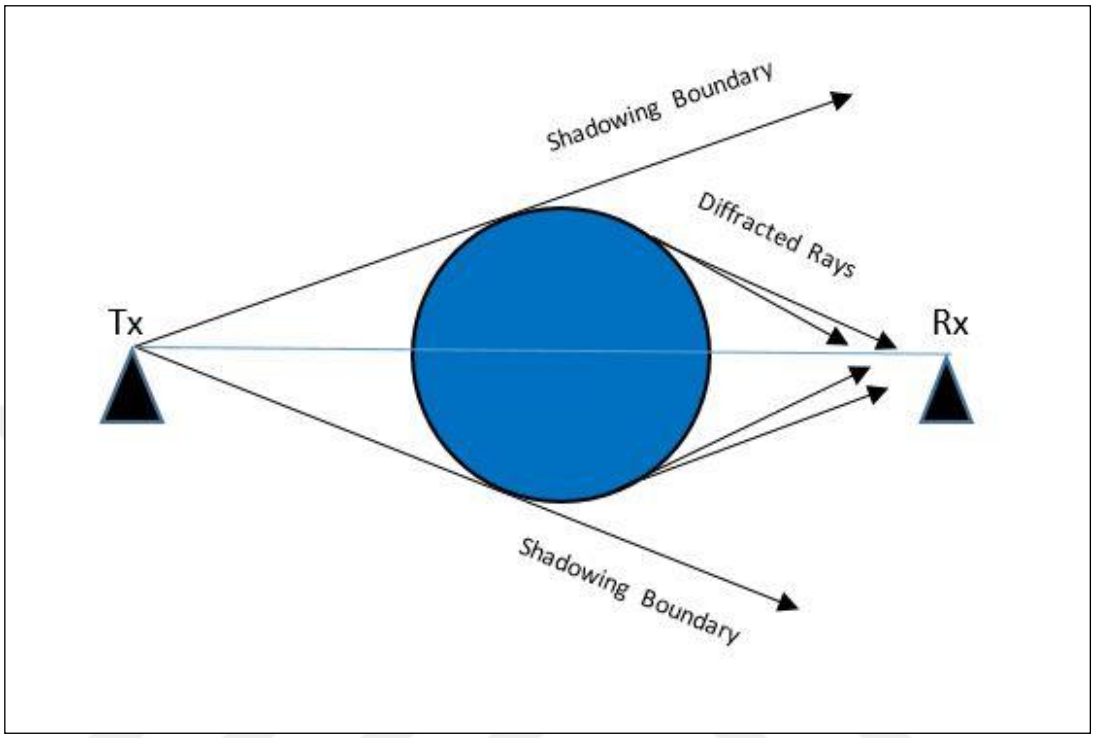

Figure 2.7: Geometric Theory of Diffraction

2.4.2.2.2 Rectangular Blade Model

Apart from the cylindrical method, for this model, human body approximated as a rectangular blade. The diffraction coefficients were taken into account for the relative angles. Thanks to its shape, this model is the most similar model to the DKED Model according to the ray formations around the human body. Furthermore, explicit ray formations around the human body provide convenience while calculating the simulations and enabling people to apply ray-tracing methods easily. The ray-tracing methods were exploited to calculate the rays traveling around the human body [33].

2.4.3 Scattering Mechanism

Another primary mechanism of propagation to comprehend the behavior of signals in the wireless channels is scattering. The scattering mechanism has the same properties with the diffraction mechanism and occurs when obstructions have relatively small dimensions according to the signal wavelength. Generally, the scattering mechanism is encountered with objects that have rough surfaces such as street signs, lamppost, and trees. Because of hitting the rough surfaces, signals are scattered in every direction.

Furthermore, these scattering objects could provide constructive effects over the received power. The surface roughness generally is evaluated by using the Rayleigh criterion. This criterion defines the critical height of the rough objects for the corresponding angles [32].

2.4.4 Ray Tracing

In wireless communication, if the propagation occurs more than one path, it is called multipath propagation. The diffraction, reflection, and scattering can create the multipath propagation, which could be either constructive or destructive for the receiver power. When considering the indoor environment with more people, we encounter multipath propagation effects depend on the scattering human bodies certainly. Accordingly, these formed new paths mean more electromagnetic waves. Moreover, more electromagnetic waves can cause more difficulties during the calculation of receiver power and obtaining the attenuation in the propagation environment. Due to computational complexity, some assumptions were considered. These were benefiting from the simple geometry instead of association with the Maxwell Equations deeply.

The approximations have been made for the site-specific conditions to predict the multipath effects in microcellular environments. During the predictions, the effects of the scattering objects and various buildings were taken into account in different frequencies. The diffraction, scattering, and reflection mechanisms were exploited during calculations.

Moreover, turning corners, reflection from walls and buildings were taken into account. The effects of them were tried to be formulated in [21] [28] [29] [30] [31]. The ray contributions over the receiver power were calculated due to the ray optical methods such as the image or pincushion method [9].

It is seen that these methods were very beneficial for predicting the effects of complicated forms of diffraction and reflection mechanisms that occurred in the environment. During the calculations of simulation results, these models benefited from the two-ray model, which is the essential method for predicting the path losses more accurately in the environments.

2.4.4.1 Multipath Ray Contributions

When propagation environment involves the various diffraction and reflection mechanisms, we have to take into account the all diffracting and reflecting elements to characterize the propagation channel.

The determined ray contributions from the image or pincushion model should be divided into the three main sub-groups. We should take into account these sub-groups for effective prediction in the propagation channel. These sub-groups as follows; rays that only contain reflection mechanism, rays that contain diffraction with or without reflection before or after, and finally rays that contain diffraction twice.

The averaged path gain of the small areas could be achieved through this classification. This classification approximated as below [9].

$$PG = \sum_i {P_R}^i + \sum_i {P_{D1}}^i + \sum_i {P_{D2}}^i \quad (2.15)$$

2.4.4.1.1 Reflection Ray

For the approximation of the rays that only include the reflection mechanisms, the reflection coefficient of each medium in the environment should be taken into account.

Furthermore, the reflection coefficients of the mediums that the electromagnetic waves propagate should be multiplied with the applied two-ray model to find the contribution of each ray.

The ray contributions are approximated by using the two-ray model on the specific direction considering the ground effects in addition to the reflection mechanism. If more than one reflection mechanism occurs, every reflection coefficient should be calculated and considered in the propagation environment while predicting the path gain. Furthermore, the reflection components of the ground and distances between the transmitter and receiver side in terms of direct ray and reflected ray also affect the path gain during the calculations, as given in Equation 2.16.

$$P_R{}^{(i)} = Po^{(i)} \prod_j \left|\Gamma_E(\theta_j)\right|^2 \tag{2.16}$$

Where θ_j, $\Gamma_E(\theta_j)$ and $Po^{(i)}$denote angle of incidence, reflection coefficient and the path gain of two-ray model. $Po^{(i)}$ can be obtained by the Equation 2.8.

2.4.4.1.2 Diffraction Ray - Diffracting Once

Unlike reflection ray contributions, we should consider the distances between transmitter source to obstruction and obstruction to the receiver source for each diffracting ray. Furthermore, we should take into account the reflection coefficients and diffraction coefficients to calculate the contributions for each ray.

As with reflecting rays, the two-ray model is essential for accurate predictions over the path gains in the propagation channel for diffracting rays. On the other hand, the transition function may be added to the formula for better approximations over the received power if necessary [9].

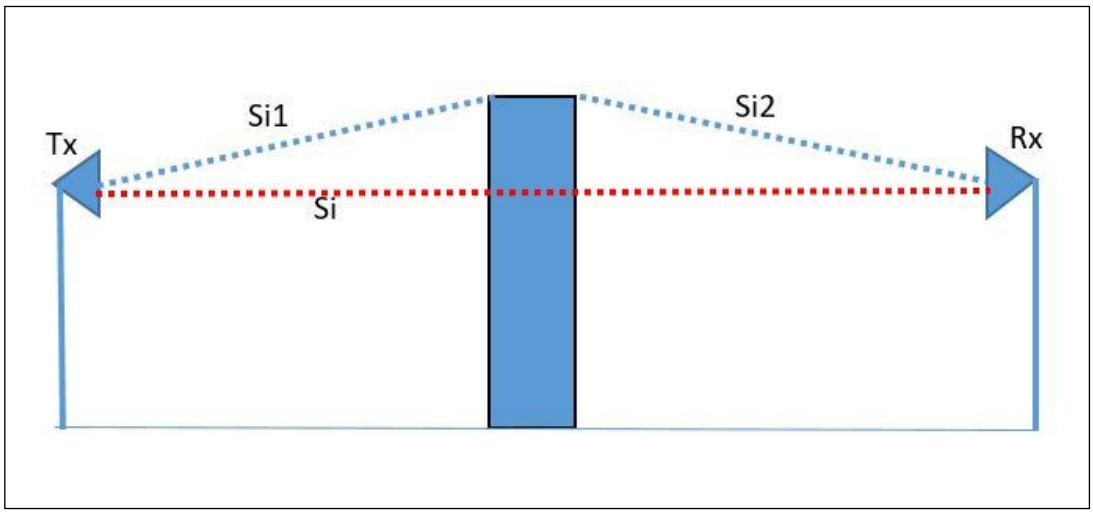

Figure 2.8: Ray contribution (diffracting once) lengths

During the calculations, the diffraction coefficient and path lengths of diffracted rays also affect the path gain as given in Equation 2.17 in addition to two-ray model components of the rays between the transmitter and receiver.

$$P_{D1}{}^{(i)} = Po^{(i)} \frac{S_i}{S_{i1}S_{i2}} |D(\theta_1)|^2 \prod_j \left|\Gamma_E(\theta_j)\right|^2 \quad (2.17)$$

Where $D(\theta_1)$ denotes the diffraction coefficient. Si_1 and Si_2 denote the unfolded path lengths from the transmitter to diffraction point and from the diffraction point to the receiver. Additionally, *Si* indicates the total unfolded ray length from transmitter to receiver, as given in Figure 2.8.

2.4.4.1.3 Diffraction Ray - Diffracting Twice

For effective prediction in the propagation channel, the sub-groups have already been divided by various ray-tracing methods. Because of this division, rays that are diffracting twice should be calculated differently from rays that are diffracting once. Both diffraction coefficients should be taken into account during the calculation of each ray, as given in Equation 2.18. Besides, the distances should be taken into account for the calculations, as given in Figure 2.9.

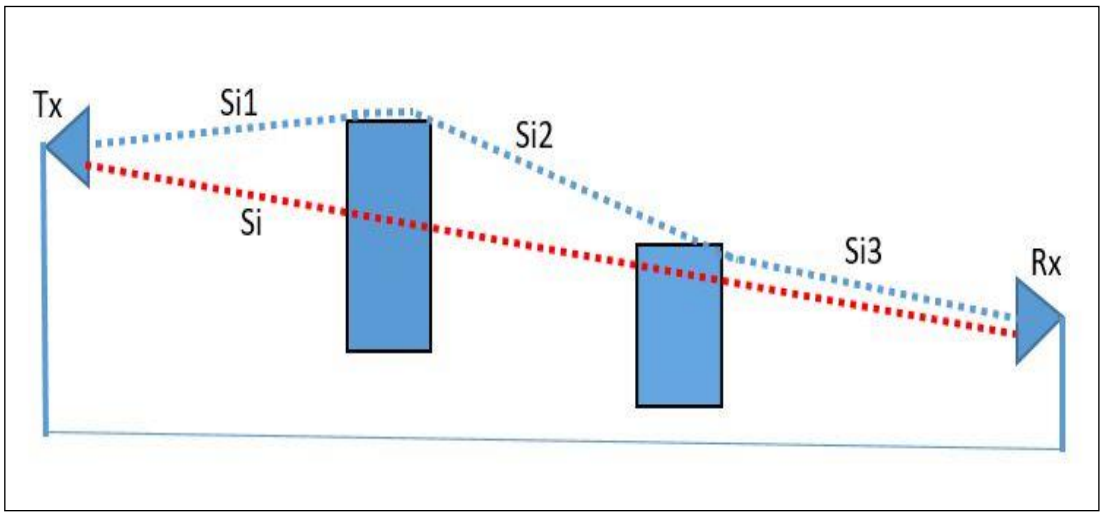

Figure 2.9: Ray contribution (diffracting twice) lengths

$$P_{D1}{}^{(i)} = Po^{(i)} \frac{S_i}{S_{i1}S_{i2}S_{i3}} |D(\theta_1)|^2 |D(\theta_2)|^2 \prod_j \left|\Gamma_E(\theta_j)\right|^2 \qquad (2.18)$$

2.5 Comparison of the Models

Because of extensive research about human body shadowing models, we concluded that the Rectangular Blade Model of GTD and the Double Knife-Edge Model are the most suitable models to characterize the propagation channel due to their accurate results. Besides, it is seen that these models are very useful to give insights about the mmWave bands, which will be allocated for the upcoming wireless technologies.

Furthermore, the diffraction rays of our models are only diffracting once in the environments. Therefore, it will be enough and convenient to employ the diffraction formulas for diffracting once for calculation of the multipath ray contributions in the rectangular blade GTD model.

CHAPTER 3

MEASUREMENT SETUP AND EXPERIMENT MODELS

In this chapter, the measurement environment is described in detail. Furthermore, some preliminary measurements that were performed to obtain accurate results are presented. For example, the antenna radiation pattern is presented, and the effects of scattering objects except the human body are determined. The measurement setup is arranged according to the corresponding scenarios. Finally, simulation models are introduced.

3.1 Measurement Setup

The measurement environment was established, and human body models were implemented in RF and Antenna Laboratory of Atilim University. The measurement setup consists of the signal generator, the spectrum analyzer with the transmitting and the receiving antennas that have identical properties. Moreover, the measurement setup is illustrated in Figure 3.1.

PE9850/2F-20 horn antennas were applied as receiving and transmitting antennas, which have the 18.3° horizontal and 16.7° vertical half-power beamwidth (HPBW) in addition to 20dBi gain. As a signal generator, the Agilent E8244A signal generator was connected to the transmitting antenna. On the other hand, the Agilent E4448A spectrum analyzer was connected to the receiving antenna through the PE3C0747-200 cables with connectors.

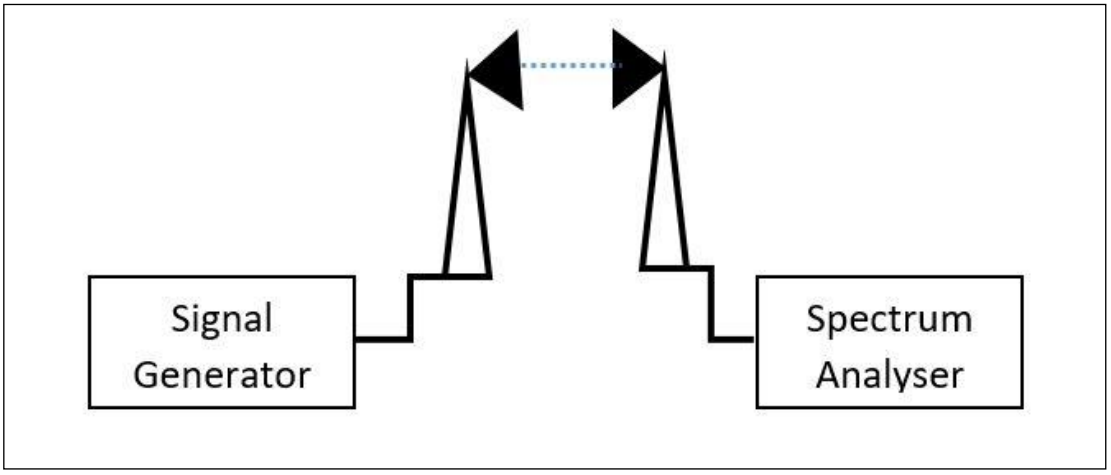

Figure 3.1: Measurement setup basics

3.2 Measurement Setup Calibration

The effects of issues such as cable losses, inconsistency over the datasheet that is indicating the antenna radiation pattern and scattering objects, excluding human bodies around the laboratory, were investigated to avoid any misleading measurement results. Accordingly, their potential effects over the receiver antenna were taken into account.

3.2.1 Floor Plan of the Laboratory

The floor plan of the laboratory is illustrated in Fig. 3.2. There were tiled wall and desks, which has 0.75 m height parallel to the link at both sides. The distances from the wall and desk to the link were 2.4 m for each. Beyond the transmitter antenna placement, there are steel cabinets, which had 2.2 m height in front of the wall. The steel cabinets were located 13.5 m far from the transmitting antenna. Besides, there was a plasterboard hanging on a tiled wall 3.0 m away from the receiving antenna. Finally, the ceiling of the laboratory room was 2.9 m height from the floor.

To calculate the multipath effects of the scattering objects around the laboratory. Works have already been done in the same environment. Some assumptions have been made about the scattering objects. During the works, the scattering objects were considered that they were the perfect conductors.

Furthermore, they were placed at predetermined positions. The received signals were measured while a human was blocking the LOS propagation between the transmitting and receiving antenna. The effects of the scattering objects were tried to be determined. Accordingly, the contributions from the scattering objects could be ignorable except human body due to the measured results. It was stated that a minimum of 14 dB isolation was observed in [12].

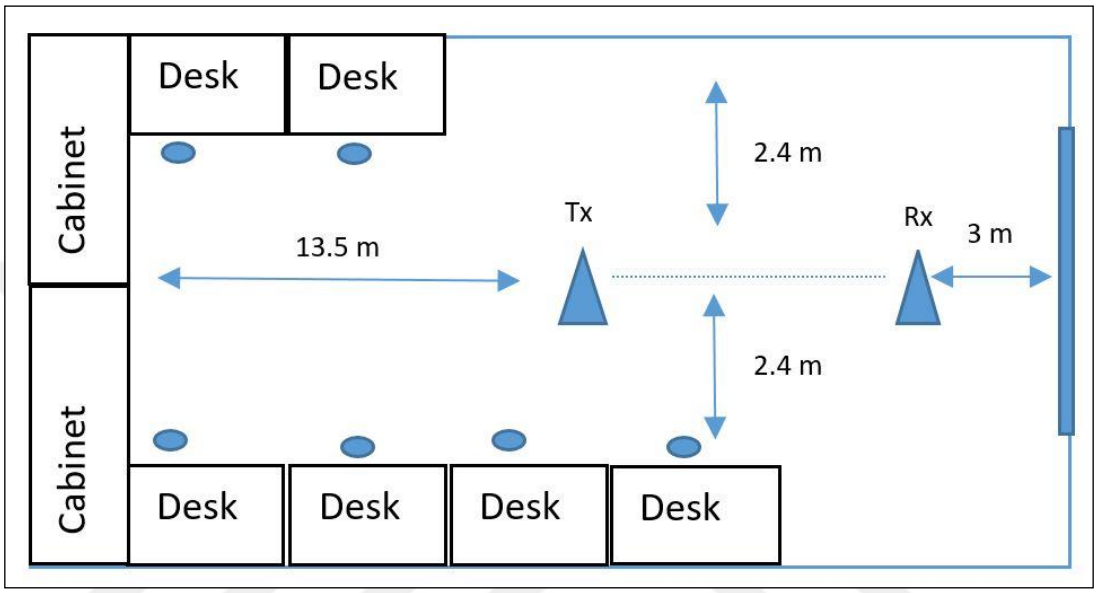

Figure 3.2: Floor plan of the laboratory

3.2.2 Antenna Radiation Pattern

The identical horn antennas were applied to the measurement setup, and some preliminary measurements were carried out to validate the antenna radiation pattern in advance. It is essential to obtain results that are more accurate during the measurements for the selected antenna polarization. For validation of radiation pattern, the measurements were taken for every 10 degrees though the created semicircle with 1.0 m radius. Besides, the measurements were conducted in the LOS path without any obstruction in the laboratory, as given in Figure 3.3. The results were compared and validated with the datasheet, which was published by the producer. The antennas were within the 2-10 dB error margin.

The results were shown in Figure 3.4 for the vertical polarization and were compatible with the previous works [12]. The horizontal plane measurements were not calculated, because all measurements, which would be done, were based on vertical polarization of the antennas.

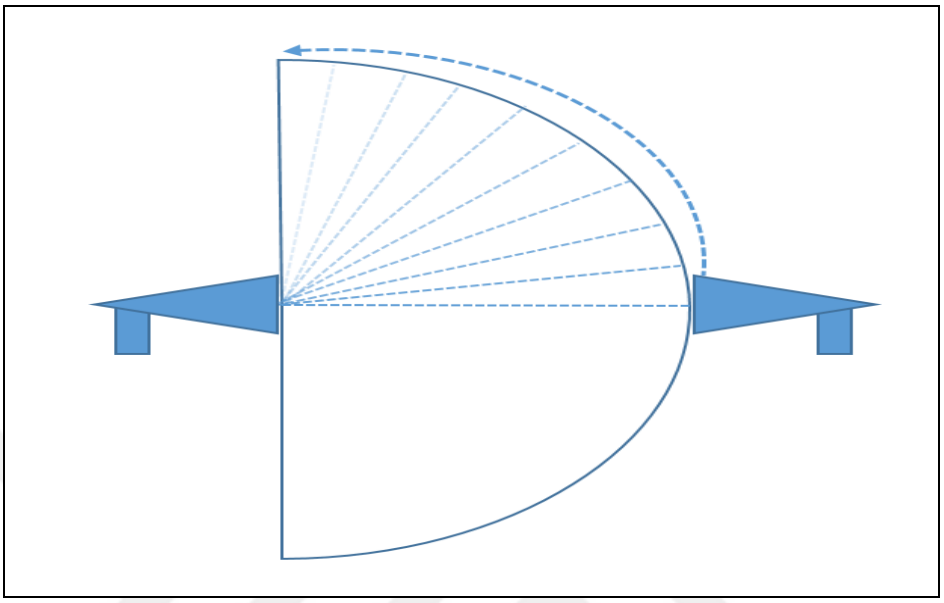

Figure 3.3: Measurement method of the antenna radiation pattern in the vertical plane

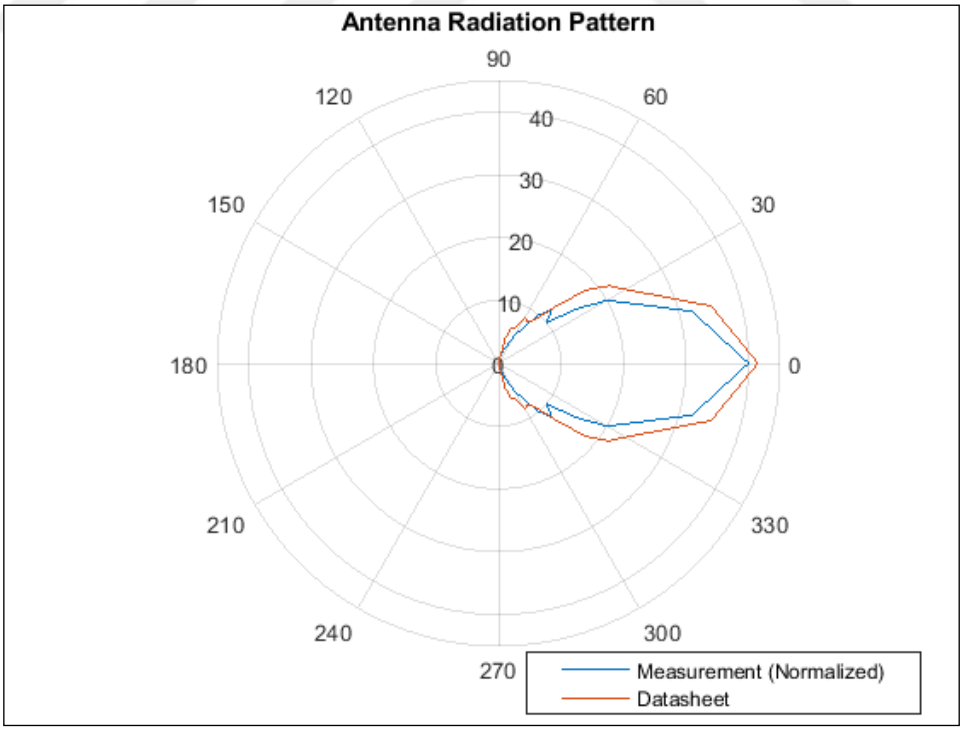

Figure 3.4: Antenna radiation pattern in the vertical plane

3.2.3 Cables and Connectors

FE3C0747LF-200CM cables were used to make the connection between the transmitting antenna to signal generator and receiving antenna to a spectrum analyzer in 28 GHz. The cable losses are extending from8.89 dB to 11.68 dB for the carrier frequencies that are ranging from 20 GHz. to 40 GHz. in the datasheet. They are representing considerable changes throughout the different carrier frequencies in mmWave. Therefore, it is seen that the mmWave bands are very susceptible to cable losses.

The measurements of calibration were conducted in the laboratory through the LOS path. The transmitter and receiver antennas were placed 1.0 m away from each other. The cable losses that depend on the carrier frequency are determined. Accordingly, it was seen that the cable losses that are indicated in the datasheet were compatible with the measurement results, which were calculated by

$$P_R(dB) = P_T(dB) + G_{Tx}(dB) + G_{Rx}(dB) - L_{total}(dB) \quad (3.1)$$

Where

$$L_{total}(dB) = FSPL(dB) + L_{cables}(dB) \quad (3.2)$$

3.3 Measurement Setup for Scenarios

3.3.1 Scenario 1: Person blocking the link while another person approaching towards the link

In this scenario, we tried to determine the effects of the approaching human body on the receiver side while another human is blocking the link completely as in [12].

In order to evaluate the effects of the scattering human bodies over the receiver side, which is significant for indoor communication systems, we deployed the two human bodies at predetermined positions around the link. The first human body was placed to the middle of the link as the blocking object, and the second human body was aligned to the first human as given in Figure 3.5.

We changed the distance between humans by changing the second human position from -0.6 m to -1.0 m with 0.1 m increments. The received power was measured for five different positions. We assumed that the human width is 0.5 m for both humans while taking into account the multiple ray contributions during the calculations of simulation models.

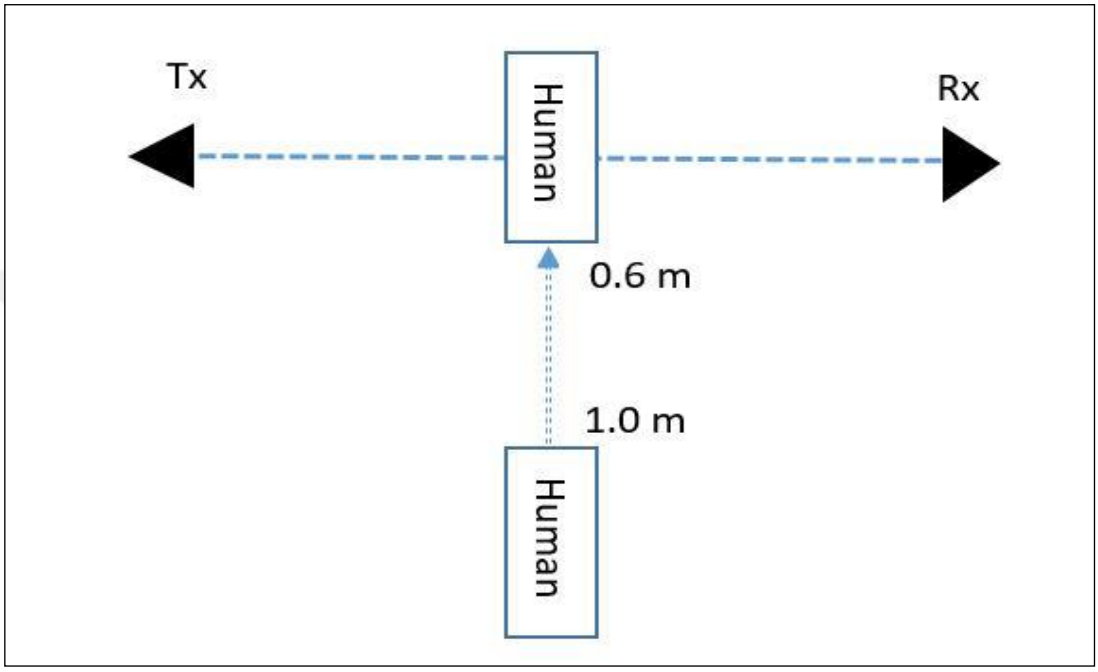

Figure 3.5: Scenario 1

3.3.2 Scenario 2: Person blocking the link while another two person approaching towards the link

In this case, we would like to see the effects of the three humans. In addition to the first scenario, we added another human, as given in Figure 3.6.

In order to evaluate the effects of the scattering human bodies over the receiver side, which is significant for indoor communication systems, we deployed the three human bodies at predetermined positions around the link. The first human body was placed to the middle of the link as blocking object, and second and third human bodies were aligned to the first human as given in Figure 3.6.

We changed the distance between humans by changing the positions of second and third human from -0.6 m to -1.0 m with 0.1 m increments together. The received power was measured for five different positions. We assumed that the human width is 0.5 m for both humans while considering the multiple ray contributions during the calculations.

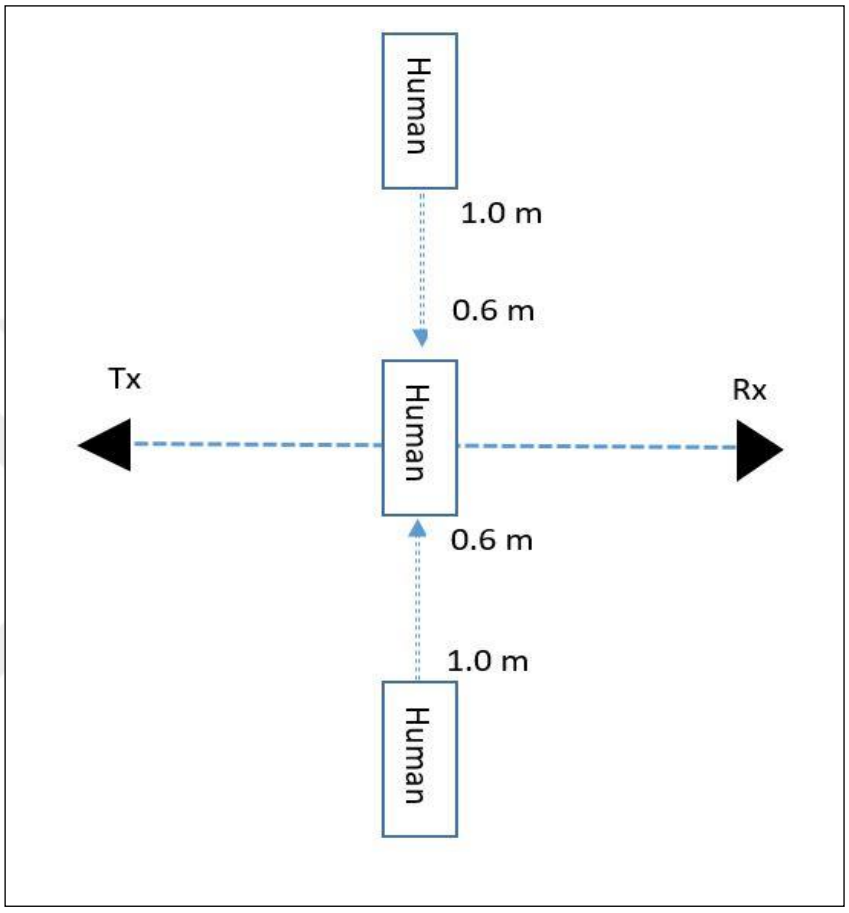

Figure 3.6: Scenario 2

3.4 Modeling of the Scattering Objects while Human Body Blocking the Link

The DKED model and The Rectangular Blade Model of GTD were applied to our human body model separately. Both of them were indicated the significant results, which could be useful for characterizing the effects of the scattering objects around the link. Besides, these simplified models could give insights about the effects of the human body at mmWave bands.

3.4.1 Double Knife-Edge Diffraction Model

We applied the DKED model, which is the modified knife-edge diffraction model while modeling both cases due to its simplicity and promising results were already obtained [12]. The DKED model consists of the infinite vertical dimension that does not allow any ray diffracting over. Furthermore, it is considered that the one diffraction ray passes in the middle of each side edges for this model. By dint of this assumption, we can eliminate the complex calculations, which are stemmed from the geometry. Besides, we can obtain insights, which indicate the effects of human bodies easily.

While calculating the Model 1 results, we benefited from Equation 2.13 and 2.14 to obtain the shadowing loss and Equation 2.2 to get the free space path loss. The product of the loss arising from the first human body and the second human body that is approaching separately, which are denoted PL1 and PL2, respectively, can express total loss.

$$Total\ Loss(dB) = P_{L1}(dB) + P_{L2}(dB) \tag{3.3}$$

Where P_{L1} and P_{L2} consist of shadowing loss and free space path loss separately,

$$PL(dB) = S_L(dB) + FSPL(dB) \tag{3.4}$$

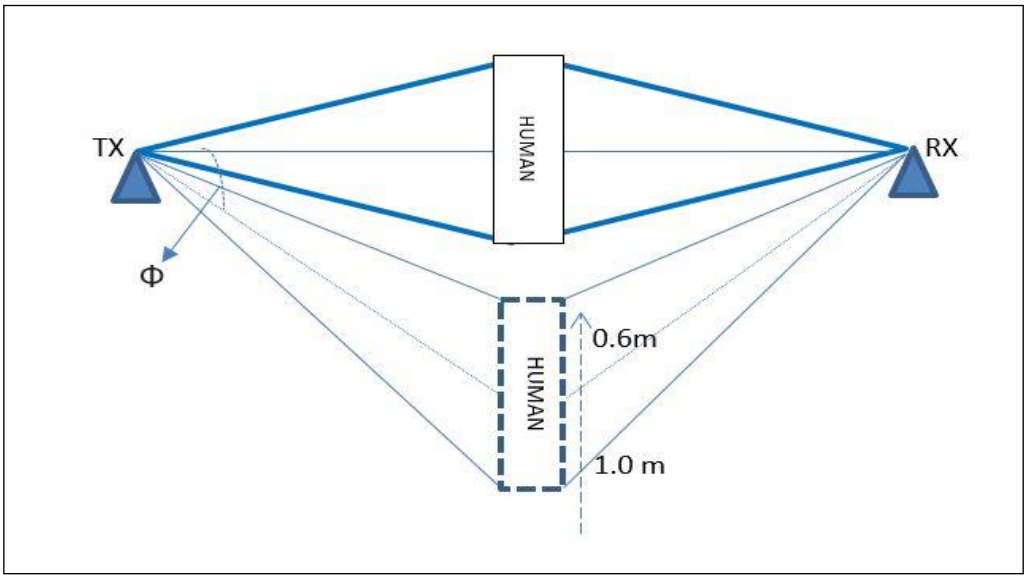

Figure 3.7: Model for scenario 1

Unlike Model 1, while calculating the Model 2 results, we benefited from the Equation 2.13 and 2.14 to obtain the shadowing loss for three human bodies and Equation 2.2 to obtain the free space path loss for three human bodies. Consequently, the product of the loss arising from the first human body, and the second and third human bodies that are approaching separately, which are denoted PL1, PL2, and PL3, respectively, can express the total loss. Meanwhile, each of them consists of the free space path loss and shadowing loss.

$$Total\ Loss(dB) = P_{L1}(dB) + P_{L2}(dB) + P_{L3}(dB) \tag{3.5}$$

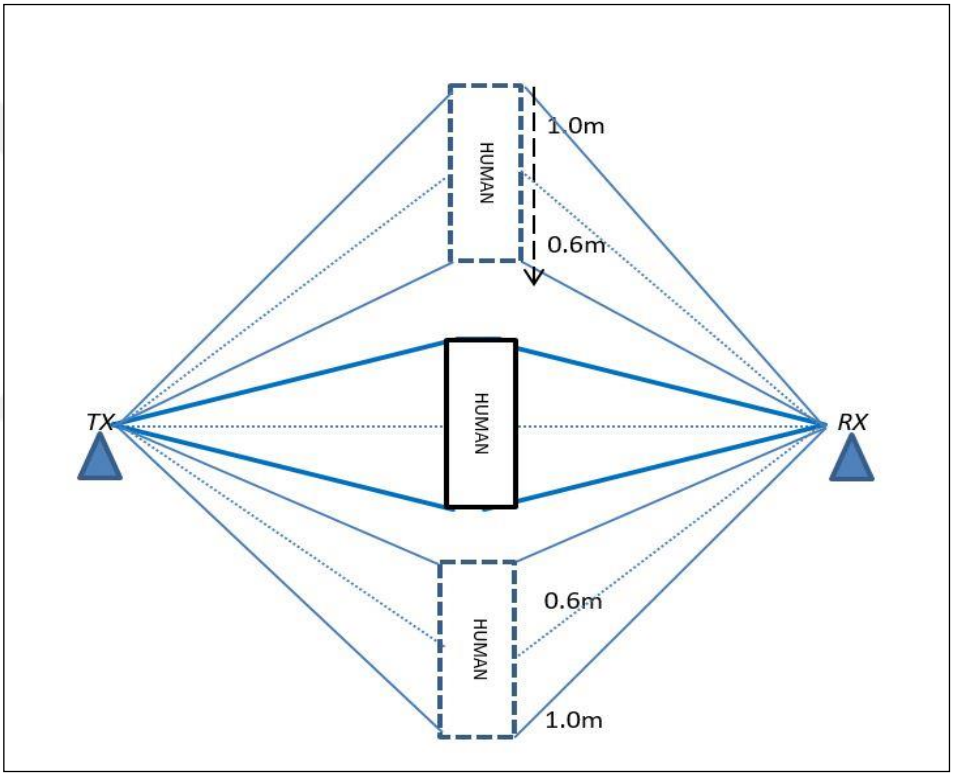

Figure 3.8: Model for Scenario 2

After obtaining the path losses and shadowing losses, we should apply the Friis formula below in order to calculate the received power.

$$P_R(dB) = P_T(dB) + G_{Tx(\Phi)}(dB) + G_{Rx((\Phi))}(dB) - L_{total}(dB) \tag{3.6}$$

3.4.2 Rectangular Blade Model of GTD

Although ray tracing with GTD was applied to obtain insights for outdoor wireless propagation in the large area networks and macro cells such as city canyons mostly, GTD is another method that is employed to our design for characterizing the propagation channel in terms of ray tracing. For both scenarios, the same geometries were arranged, which were given in Figure 3.7 and Figure 3.8 to obtain the GTD model results. Furthermore, the human bodies were assumed as a rectangular blade. It was considered that only two rays travel around the rectangular blades. For the sake of simplicity, these rays are considered diffracting from the points of edges 1.0 m above from the ground.

Besides, diffraction coefficients were obtained using the formula, which aims to calculate the diffraction coefficients for absorbing screens due to the rough surface of the dress and cloths.

$$D(\theta_i) = \frac{-1}{\sqrt{2\pi k}}\left[\frac{1}{\theta_i} + \frac{1}{2\pi - \theta_i}\right] \tag{3.7}$$

Moreover, it was observed that our models only consist of the diffracted rays, which diffracted once over the human bodies. Accordingly, we applied the corresponding formula in Equation 2.17, which was derived from the classification of the diffracted rays in Equation 2.15. Furthermore, the two-ray model was exploited to each ray to obtain the average path gain of small area for more realistic results during the calculations.

CHAPTER 4

MEASUREMENT RESULTS

In this chapter, the simulation results of the DKED Model and the Rectangular Blade Model of GTD were compared with the laboratory measurement results. These results were examined in order to evaluate the accuracy of the models for the characterizing of multiple human bodies. Consequently, the comparisons are presented for scenarios.

4.1 Scenario 1: Person blocking the link while another person approaching towards the link

The simulation results of the Rectangular Blade Model of GTD and DKED model were obtained by using relevant calculations. Furthermore, these results were compared with the laboratory measurement results for Scenario 1 in Figure 4.1. The measurement and model results of DKED obtained for this scenario were validated by comparison with the previous study results [12].

MODEL / POSITION	Rectangular Blade Model of GTD (dB)	DKED Model (dB)	Measurement (dB)
-0.6 m	**0**	**0**	**0**
-0.7 m	**-2.06**	**-5.2**	**-2.2**
-0.8 m	**-3.61**	**-5.9**	**-2.3**
-0.9 m	**-6.61**	**-7.0**	**-2.6**
-1.0 m	**-9.86**	**-8.6**	**-5.0**

Table 4.1: Comparison of measurements and models for Scenario 1

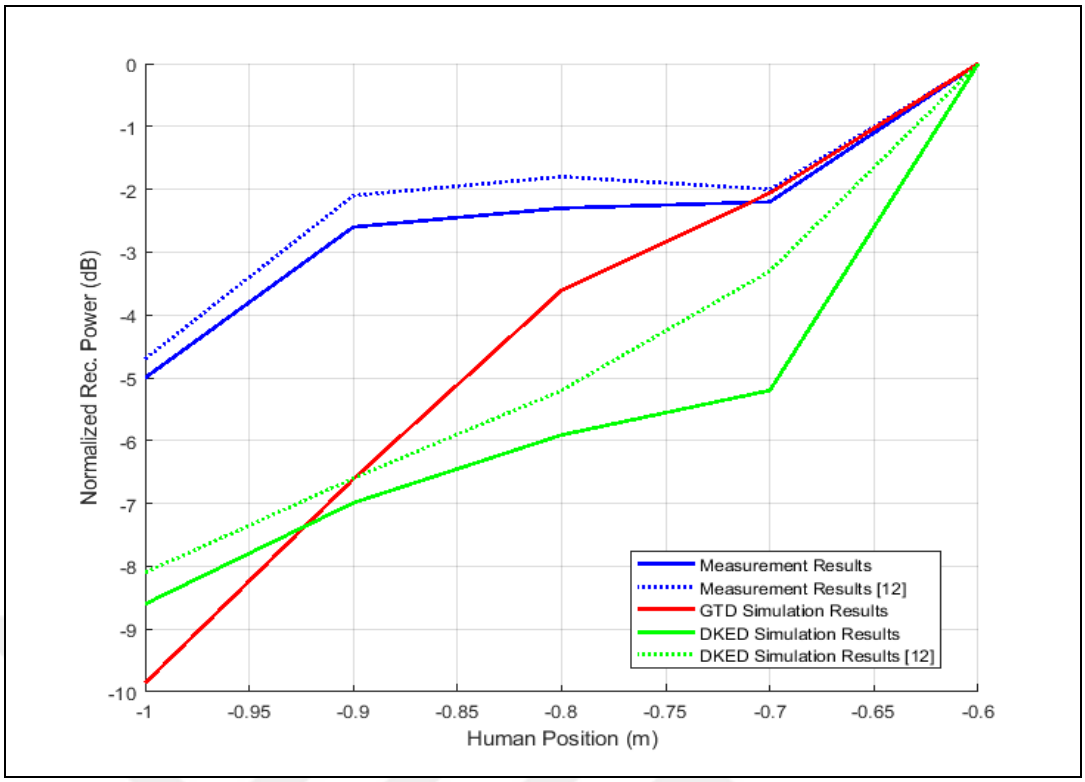

Figure 4.1: Comparison of measurements and models for scenario 1

For scenario 1, It was seen that results are compatible and differences are less than 1 dB with the previous study [12] in the context of DKED model and laboratory measurement.

Besides, it is seen that the simulation results of the DKED model exceed the measurement results in all distances. The DKED model is inconsistent with approximately 3.0 dB at -0.7 m distance, and then inconsistency reaches approximately 3.6 dB at -1.0 m distance. On the other hand, it is seen that the simulation results of the Rectangular Blade Model of GTD exceed the measurement results after -0.7 m distance. The Rectangular Blade Model of GTD is consistent only at -0.7 m distance. However, this model is inconsistent at the distances after -0.7m. The inconsistency occurs and increases for further distances. Accordingly, it also exceeds the simulation results of the DKED model and reaches approximately 4.86 dB difference at -1.0 m. Both models seem enough to characterize the effects of human bodies as scattering objects in the environments, and inconsistencies can be ignored.

Consequently, the results have indicated the inconsistency between simulations and measurements of approximately 3-5 dB. The inconsistency may stem from the simplified models were employed. It is already known that the simplified models do not take into account all properties of the wave propagation during the calculation of simulation results.

Besides, the DKED model is compatible with the measurement results, as in [12]. The results of the Rectangular Blade Model of GTD are getting unmatching than the DKED model for the distances away from the link gradually.

4.2 Scenario 2: Person blocking the link while another two person approaching towards the link

The Rectangular Blade Model of GTD and DKED model simulation results were obtained by using relevant calculations. Furthermore, these models were compared with the laboratory measurement results for Scenario 2 in Figure 4.2.

MODEL / POSITION	Rectangular Blade Model of GTD (dB)	DKED Model (dB)	Measurement (dB)
-0.6 m	**0**	**0**	**0**
-0.7 m	**-2.74**	**-6.9**	**-3.3**
-0.8 m	**-4.80**	**-7.8**	**-4.0**
-0.9 m	**-8.81**	**-9.3**	**-6.1**
-1.0 m	**-13.14**	**-11.4**	**-7.8**

Table 4.2: Comparison of measurements and models for Scenario 2

For scenario 2, it is seen that the simulation results of the DKED model exceed the measurement results in all distances. The DKED model is inconsistent with approximately 3.6 dB at -0.7 m distance, and then inconsistencies seem similarities for further distances.

On the other hand, it is seen that the simulation results of the Rectangular Blade Model of GTD exceed the measurement results at -0.8 m distance. Furthermore, this model is inconsistent at the distances after -0.7 m. The inconsistencies occur and increase for further distances. Accordingly, it exceeds the simulation results of the DKED model and reaches approximately 5.34 dB difference at -1.0 m.

Both models seem enough to characterize the effects of human bodies as scattering objects in the environments, and inconsistencies can be ignored. The results indicate the inconsistency between the simulations and measurements, which may stem from using simplified models, which were employed as in the other scenario.

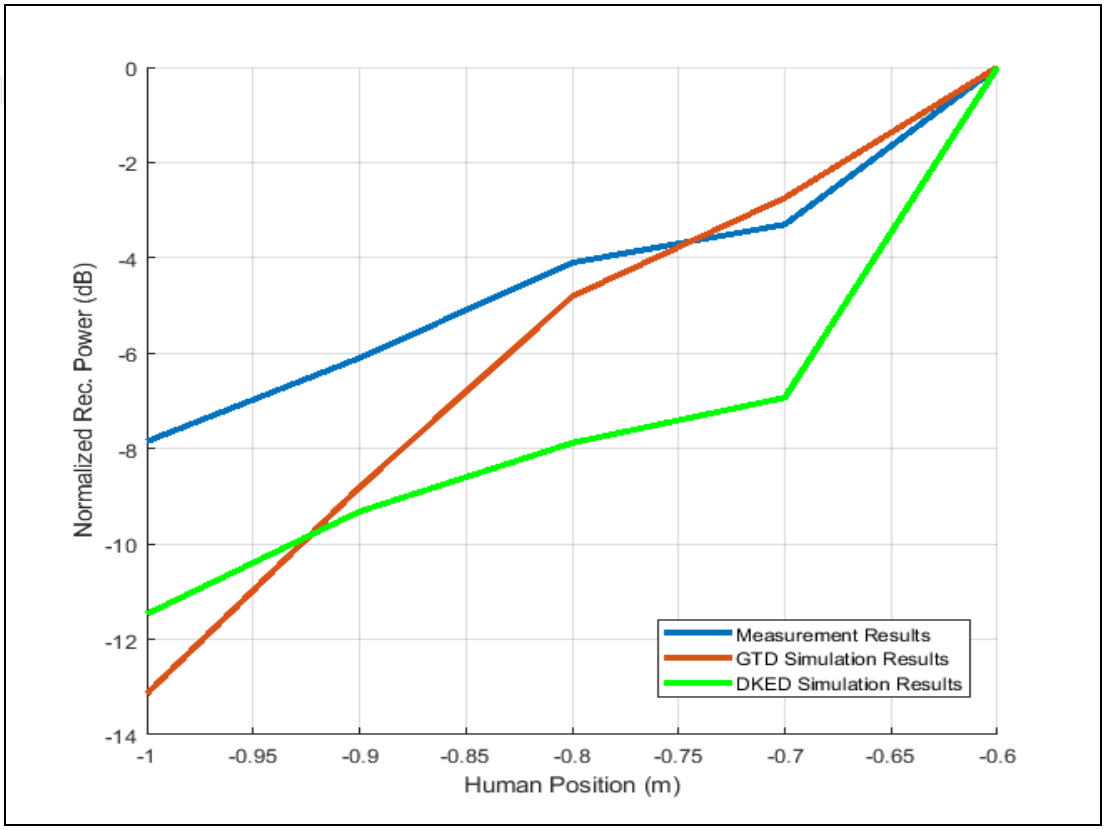

Figure 4.2: Comparison of measurements and models for scenario 2

In addition, our simulation results are compatible with the study that has presented the comparison of human body models in detail. Accordingly, the differences that were obtained from the simplified models are consistent with the study [33].

CHAPTER 5

CONCLUSIONS

This thesis aims to represent the effects of the multiple human bodies as scattering objects for indoor environments while another human body is entirely blocking the link between the receiver and transmitter at 28 GHz.

Currently, millimeter-wave bands consist of a suitable vast amount of frequency bands, which could be utilized for 5G because of unsuitable reallocation in the lower frequencies. To characterize the effects is significant while designing the systems that use millimeter-wave bands due to their extremely affected nature from the environmental issues. Various simplified human body models were investigated to characterize the changes over the received power due to the scattering human bodies. Accordingly, DKED and GTD models were applied for the simulations due to their prediction accuracy and simplicity. The results of the simulation of models and the laboratory measurements were compared for each corresponding scenario. The simulation of the DKED model for scattering multiple human bodies indicated well-matched results with the measurements. On the other hand, the rectangular blade model of GTD, which exploits from the ray-tracing, displayed similar results with slightly unmatching than the DKED model for each scenario. The compatible results were observed after comparing both models with laboratory measurements.

The inconsistencies over received power between the measurement and models were considered deriving from the antenna gain pattern or stemming from human geometry, which presumably more effective in simulations than laboratory measurements. DKED model can be seen as the most suitable simplified model for characterizing the attenuation over the received power.

Accordingly, the DKED model and the Rectangular Blade model of GTD could be beneficial to give accurate insights about the effects of human body shadowing for various indoor environments that will be deployed by 5G networks in the future.

Consequently, 24.25-27.5 GHz., 37-43.5 GHz., 45.5-47 GHz., 47.2-48.2 GHz, and 66-71 GHz. in the mmWave are allocated for wireless systems [5]. The studies within the frame of this thesis could be developed for these allocations. The simplified models could be extended to characterize the effects of multiple human bodies for different deployments.

REFERENCES

[1] O.T. Eluwole, N. Udoh, M. Ojo, C. Okoro and A. J. Akinyoade, "From 1G to 5G, what next?" IAENG International Journal of Computer Science (IJCS), vol.45, no.3, pp. 413-434, 2018.

[2] Y. Niu, Y. Li, D. Jin, L. Su, and A. V. Vasilakos, "A survey of millimeter wave communications (mmWave) for 5G: opportunities and challenges." Wireless Netw. vol.21, no.8, pp. 2657–2676, 2015.

[3] I.F. Akyildiz, S. Nie, S. Lin, and M. Chandrasekaran, "5G roadmap: 10 key enabling technologies." Computer Networks Vol.106, pp.17-48, 2016.

[4] M. Taheribakhsh, A. Jafari, M. M. Peiro and N. Kazemifard, "5G Implementation: Major Issues and Challenges." in International Computer Conference, Computer Society of Iran (CSICC), pp.1-5, 2020.

[5] World Radiocommunication Conference 2019 (WRC-19), Final Acts, 2019

[6] A. N. Uwaechia and N. M. Mahyuddin, "A Comprehensive Survey on Millimeter Wave Communications for Fifth-Generation Wireless Networks: Feasibility and Challenges." IEEE Access, vol. 8, pp. 62367-62414, 2020.

[7] T. Rappaport, Y. Xing, G. R. MacCartney, A. F. Molisch, E. Mellios and J. Zhang, "Overview of millimeter wave communications for fifthgeneration (5G) wireless networks-with a focus on propagation models." IEEE Trans. Antennas Propag., vol. 65, no. 12, pp. 6213–6230, Dec. 2017.

[8] T. S. Rappaport et al., "Millimeter wave mobile communications for 5G cellular: It will work!" IEEE Access, vol. 1, pp. 335–349, May 2013.

[9] H. L. Bertoni, Radio propagation for modern wireless systems, Pearson Education, 1999.

[10] A. Kara, "Human body shadowing variability in short-range indoor radio links at 3-11 GHz band." Int. J. Electron., vol. 96, no. 2, pp. 205-211, 2009.

[11] J. S. Lu, D. Steinbach, P. Cabrol, and P. Pietraski, ''Modeling human blockers in millimeter wave radio links,'' ZTE Commun., vol. 10, no. 4, pp. 23–28, Dec. 2012.

[12] Y. Dalveren, A. H. Alabish, and A. Kara, "A Simplified Model for Characterizing the Effects of Scattering Objects and Human Body Blocking Indoor Links at 28 GHz." IEEE Access, vol.7, pp. 69687-69691, 2019.

[13] M. Nakamura, M. Sasaki, W. Yamada and Y. Takatori, "Path Loss Model in Crowded Indoor Environments Considering Multiple Human Body Shadowing of Multipath at 4.7 GHz and 66.5 GHz." 13th European Conference on Antennas and Propagation (EuCAP), pp. 1-5, 2019.

[14] M. Nakamura, M. Sasaki, M. Inomata and Y. Takatori, “Path-loss prediction considering human-body shadowing of multi-path components in crowded area at 4.7 and 26.4 GHz.” 2017 International Symposium on Antennas and Propagation (ISAP), pp. 1-2, Phuket, 2017,

[15] X. Chen, L. Tian, P. Tang, J. Zhang, “Modeling of human body shadowing based on 28 GHz indoor measurement results.” in Proc. VTC-Fall, Montreal, QC, Canada, pp. 1-5, Sep. 2016.

[16] P. Karadimas, B. Allen, and P. Smith, “Human body shadowing characterization for 60-GHz indoor short-range wireless links.” IEEE Antennas Wireless Propag. Lett., vol. 12, pp. 1650-1653, 2013.

[17] G. R. MacCartney, S. Deng, S. Sun, and T. S. Rappaport, “Millimeterwave human blockage at 73 GHz with a simple double knife-edge diffraction model and extension for directional antennas.” in Proc. VTC-Fall, pp. 1-6. Sep. 2016,

[18] M. Umehira, S. Takeda, T. Miyajima and K. Kagoshima, “An extended calculation model for shadowing loss caused by a moving human body in 60 GHz WLAN.” in The 20th Asia-Pacific Conference on Communication (APCC2014), pp. 113-116, 2014.

[19] M. Ghaddar, L. Talbi, T. A. Denidni, and A. Sebak, “A conducting cylinder for modeling human body presence in indoor propagation channel.” IEEE Trans. Antennas Propag., vol. 55, no. 11, pp. 3099-3103, Nov. 2007.

[20] Y. Dalveren, and A. Kara, “Examining the Effects of Human Bodies Blocking Indoor Links at 28 GHz with a Perfectly Conducting Cylinder Model.” Düzce University Journal of Science & Technology, vol.8 no.1 pp. 1118-1127, 2020.

[21] J. S. Lu, H. L. Bertoni, K. A. Remley, W. F. Young, and J. Ladbury, ”Site-Specific Models of the Received Power for Radio Communication in Urban Street Canyons.” IEEE Trans. Antennas Propag., vol. 62, no. 4, 2014.

[22] “Patterns and trends in household size and composition: Evidence from a United Nations dataset.” Department of Economic and Social Affairs Population Division, 2019.

[23] S. Haykin, and M. Moher, Modern wireless communications. Pearson Education, 2005.

[24] P. Pagani and P. Pajusco, “Characterization and modeling of temporal variations on an ultrawideband radio link.” IEEE Trans. Antennas Propag., vol.54, pp. 3198-3206, 2006.

[25] H. Hosseinianfar, J. Lian, and M. Brandt-Pearce, “Probabilistic Shadowing Model for Indoor Optical Wireless Communication Systems.” 53rd Asilomar Conference on Signals, Systems, and Computers, pp. 936-941, 2019.

[26] G. L. James, Geometrical theory of diffraction for electromagnetic waves. IET, 1986.

[27] METIS 2020, “METIS Channel Model.” Tech. Rep. METIS 2020, Deliverable D1.4 v3, July 2015.

[28] F. Niu and H. L. Bertoni, “Path loss and cell coverage of urban microcells in high-rise building environments,” in Proc. IEEE Global Telecommun. Conf. (GLOBECOM), vol. 1, pp. 266-270, 1993.

[29] G. E. Athanasiadou, A. R. Nix, and J. P. McGeehan, “A microcellular ray-tracing propagation model and evaluation of its narrow-band and wide-band predictions.” IEEE J. Sel. Areas Commun., vol. 18, no. 3, pp. 322-335, 2000.

[30] Z.-Y. Liu, T.-L. Zhang, L.-X. Guo, and J. Li, “Effects of Diffraction and Ground Reflection on Ray Tracing-Based Coverage Predictions in Urban Microcellular Environments.” Cross Strait Quad-Regional Radio Science and Wireless Technology Conference (CSQRWC2018), pp. 1-3, 2018.

[31] K. Rizk, J. F. Wagen, and F. Gardiol, “Two-dimensional ray-tracing modeling for propagation prediction in microcellular environments.” IEEE Trans. Veh. Technol., vol. 46, no. 2, pp. 508-518, May 1997.

[32] T. S. Rappaport, Wireless communications: principles and practice vol. 2. Prentice hall PTR, 1996.

[33] A. D. C. de Queiroz and L. C. Trintinália, “An analysis of human body shadowing models for ray-tracing radio channel characterization.” SBMO/IEEE MTT-S International Microwave and Optoelectronics Conference (IMOC), pp. 1-5, 2015.

[34] J. B. Keller, Geometrical Theory of Diffraction, J. Opt. Soc. Am. 52, 116-130 1962.

[35] A. Goldsmith, Wireless communications. Cambridge University Press, 2012.